Applied Thermal Engineering 196 (2021) 117322

Contents lists available at ScienceDirect

Applied Thermal Engineering

journal homepage: www.elsevier.com/locate/apthermeng

The influence of aspect ratio on the thermal performance of a cryogenic pulsating heat pipe

J.M. Pfotenhauer [a,*], X. Sun [a,b], A. Berryhill [c], C.B. Shoemaker [c]

[a] Department of Mechanical Engineering, University of Wisconsin-Madison, Madison 53706, USA
[b] Institute of Refrigeration and Cryogenics, Zhejiang University, Hangzhou 310027, China
[c] Cryomagnetics, Inc, Oak Ridge, TN 37830, USA

ARTICLE INFO

Keywords:
Pulsating heat pipe
Aspect ratio
Helium
Hydrogen

ABSTRACT

Pulsating heat pipes (PHPs) are expected to serve as a significant design component for the thermal management of superconducting magnets and various cryogenic space applications, including cryogen storage tanks and low temperature detectors on telescopes. A growing body of data is accumulating regarding the performance of cryogenic PHPs, including operation with helium, hydrogen, neon, and nitrogen, and the notable dependence on their orientation with respect to gravity. However, in view of the expectation that the thermal path between a low temperature heat source and the corresponding cryocooler will involve a convoluted route including vertical, horizontal, and sloping segments, we have begun a systematic study regarding the influence of the vertical-to-horizontal aspect ratio of a PHP on its thermal performance. Although various studies available in the literature characterize the performance of completely vertical or completely horizontal PHPs, this study quantitatively displays the relative impact of the vertical and horizontal segments on the performance of a mixed orientation PHP. This systematic investigation is the first of its type to characterize the influence of the vertical-to-horizontal aspect ratio of a PHP on its thermal performance. Data gathered with both helium and hydrogen filled PHPs including five different aspect ratios confirm the expectation that vertically dominated geometries perform better than horizontally dominated geometries. Minimum thermal resistance values ranging from 1.5 K/W to 20 K/W for the 1-meter-long PHPs, with aspect ratios varying from 4:1 to 1:4, are reported as a function of heat load, fill ratio, and fluid type. Here the aspect ratio is defined by the length of the vertical adiabatic section divided by the length of the horizontal adiabatic section. The results with the hydrogen PHP demonstrate that a fill ratio of 70% significantly reduces the influence of orientation and heat load on the PHP's thermal resistance. The combined results provide valuable guidance for their application as heat transfer components in superconducting magnets and various cryogenic space applications.

1. Introduction

Cryogenic pulsating heat pipes present attractive features for application as strategic heat transfer components in the design and operation of superconducting magnet systems. Indeed, some of the earliest reports of cryogenic PHPs describe their motivation for investigating the performance of PHPs in the low temperature regime based on their potential application as effective heat transfer devices for superconducting magnets [1–3].

Two features of the PHP make them attractive for application in superconducting magnet designs. The first is their very effective heat transfer characteristic. Prior to the 1990s, superconducting magnets were commonly cooled to their required operating temperature by using a liquid cryogen, either via a liquid bath or a forced flow cooling approach [4]. Since 1990, the continual and significant improvements in cryocooler technology have provided attractive alternatives for cooling superconducting magnets [5]. For example, one needs only to supply electrical power to the cryocooler and, dependent on the make and model, cooling power at associated temperatures from 1 to 2 W at 4 K, up to 600 W at 80 K are available [6]. An increasing number of superconducting magnet designs have migrated toward a 'dry' approach in which the necessary cooling is provided by a mechanical cryocooler (see for example [7,8]). However, the most commercially available and convenient cryocoolers provide their cooling power at the spatially

* Corresponding author.
E-mail address: pfot@engr.wisc.edu (J.M. Pfotenhauer).

https://doi.org/10.1016/j.applthermaleng.2021.117322
Received 5 January 2021; Received in revised form 30 June 2021; Accepted 1 July 2021
Available online 7 July 2021

constrained location of the cryocooler cold tip [6,9–10]. Distributing the cooling power from the cryocooler cold tip with a typical surface area of 0.01 m^2 to cool a magnet structure with multiple square meters of surface area is a challenge and most commonly accomplished via conduction through high purity metals (copper or aluminum). However, as demonstrated in the example provided in Fig. 1, effective heat transfer between the cryocooler and the magnet requires significant quantities of the high purity metals, and effective heat transfer is crucial because of the strongly temperature-dependent superconducting properties.

Because the current density that can be carried by a superconductor, and the corresponding magnetic field strength that it can produce, decreases sharply as its operating temperature increases (see for example Wilson [4] section 5.2) it is important that the temperature difference between the magnet and the cryocooler be as minimal as possible. As detailed by Dresner, the temperature difference should be close to or less than 1 K [11].

As a result, conduction-cooled dry magnets frequently incorporate high purity metallic components that are massive, expensive, and inefficient; they require significant time for the magnet to cool down from room temperature to its cryogenic operating temperature (see for example pgs. 229–232 in Iwasa [12]). The large mass is prohibitive for space-borne applications, and at the least, awkward even for ground-based magnets. PHPs exhibit an effective thermal conductivity more than an order of magnitude larger than high purity metals such as copper and aluminum. They can therefore be utilized to reduce cold mass and effectively transfer heat from the magnet system components such as the magnet winding, thermal shields, and current leads, to cryocoolers or even cryogen reservoirs.

Fig. 1 displays an example of a superconducting magnet utilizing high purity copper bus bars to distribute the cooling power from the cold fingers of four cryocoolers to the key components of the superconducting magnet system. The symmetry of the magnet makes possible duplicate cooling systems at each end. For perspective, the overall dimensions of the SCU system shown are 1.75 m long, 1.25 m tall, and 0.55 m wide. The copper bus route labeled ‘a’ includes two horizontal lengths of 0.18 m and 0.1 m as well as a 0.12 m length at an angle of 45 degrees away from vertical. The approximate total mass of copper in bus route ‘a’ is 7.2 kg. The copper bus route labeled ‘b’ includes a horizontal length of 0.27 m, a vertical length of 0.16 m, and an approximate total mass of 8.6 kg. The thermal resistance of each bus at 4 K is 0.055 K/W for bus a, and 1.2 K/W for bus b.

PHPs present an attractive alternative as a low-mass thermal bus for such a superconducting magnet system. However, before they can be included in the design process, it is crucial to first characterize their thermal performance, because it is impacted by the combined vertical and horizontal path they must extend between the cryocooler and the object being cooled (in this case the liquid helium reservoir).

The second attractive feature is the small cross section of the capillary tubes comprising the PHP. Not only can the PHP replace large, bulky sections of high purity metals required to provide the same thermal conductance, but the capillary size also provides the possibility for the heat transfer to be integrated into the superconducting winding – precisely in the location where it is crucial to remove any heat source - without significantly degrading the valuable overall current density of the magnet [1].

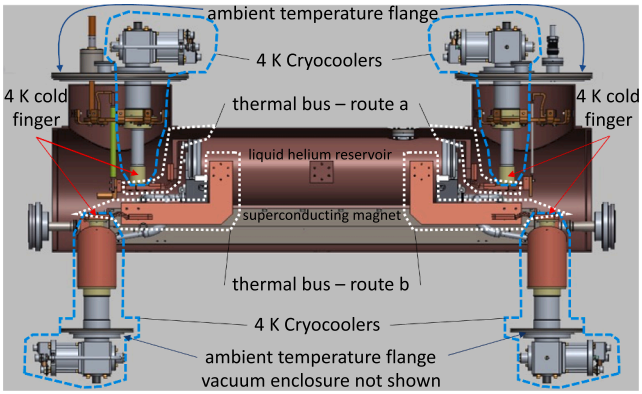

Fig. 1. Cutaway view showing the cooling system for the superconducting undulator magnet at Argonne National Laboratory [13].

The PHP’s remarkable heat transfer properties, operative primarily between the fluid’s triple point and critical point, limit their useful temperature range to roughly less than 5 K for helium, 14 K to 33 K for hydrogen, 25 K to 44 K for neon, 55 K to 154 K for oxygen, 64 K to 126 K for nitrogen, 84 K to 150 K for argon, and 89 K to 190 K for methane. In many superconducting magnet systems, thermal shields tied to the intermediate temperatures provided by a cryocooler’s upper stage provide the advantage of reducing the heat load impinging on the coldest components of the magnet [13]. In this way, the magnet operating near 4 K and surrounded by a shield, held for example at 25 K, will receive a thermal radiation load proportional to $(25)^4$ in accordance with the Stefan Boltzmann law [14]. The much larger thermal radiation load emanating from the room temperature enclosure at 300 K, and proportional to $(300)^4$ is received by the thermal shield. With such a standard configuration in mind, one may observe that a superconducting magnet system can also benefit from the remarkable heat transfer property of a PHP when it is connected between the thermal shield and the upper stage of the cryocooler, and it is filled with a cryogen whose operating range falls in the corresponding temperature range. In the present study a superconducting undulator magnet designed to operate in the 3 K to 4 K range incorporates a thermal shield operating in the 20 K to 30 K range. PHPs utilizing helium and hydrogen are therefore appropriate thermal transport components to investigate for such a superconducting magnet system.

The remarkable thermal performance documented for a helium PHP is reflected by effective thermal conductivity values ranging as high as 50,000 W/m-K to 150,000 W/m-K [15]. Effective thermal conductivity values for hydrogen PHPs range between 50,000 W/m-K and 70,000 W/m-K [16]. Nevertheless, for the purpose of moving heat between the magnet or thermal shield and the cryocooler a more significant metric for the PHP is the thermal conductance (or thermal resistance). In such a case, one recognizes that due to the small cross section of the capillary tubes making up the PHP, tens of parallel tubes are required to effectively transfer the heat while maintaining the temperature difference between the warm and cold ends to less than 1 K. Furthermore, the remarkable performance values are usually associated with the PHP in a vertical orientation with the heat source below the heat sink. Unlike PHPs operating in the room temperature regime for which the influence of orientation with respect to gravity can be reduced by increasing the number of turns beyond 20 [17], the influence of orientation with respect to gravity for cryogenic PHPs displays no reduction as the number of turns is increased [18]. We conjecture that the strong sensitivity with respect to orientation may be attributed to the relatively small values of viscosity for the cryogens as compared to the room temperature fluids. Whereas the viscosity of water is on the order of 1000 μPa-s, for neon it is ~ 100 μPa-s, for hydrogen ~ 10 μPa-s and for helium ~ 4 μPa-s. Cryogenic PHPs in a fully horizontal orientation exhibit a conductance reduced roughly by a factor of two or more compared to the same PHP in a fully vertical orientation [1,19].

The series of publications by the Japanese group at the National Institute for Fusion Science in Toki, Japan [1–3] one of the earliest groups to explore the use of cryogenic PHPs for cooling superconducting magnets, describe the performance of hydrogen, neon and nitrogen PHPs as a function of heat load, filling ratio, and orientation. They demonstrate that a 4-turn PHP filled with hydrogen provides an effective thermal conductivity on the order of 10 kW/m-K in the vertical orientation with the evaporator at the bottom, and that this value decreases by approximately half in the horizontal orientation [3]. Furthermore, they find that the PHP does not operate at all if the condenser is at a

lower elevation than the evaporator. Similar behavior is demonstrated for the neon-filled PHP but with a maximum effective thermal conductivity closer to 20 kW/m-K [3].

The same interest of applying cryogenic (neon) PHPs to cool superconducting magnets is presented in a sequence of publications from Liang, Li & Wang [20–22]. The orientation of their PHPs is primarily vertical; however, a complimentary article from M. Barba *et al* [23] exploring a long-length horizontal neon PHP provides a useful comparison for the purpose of assessing the influence of orientation on the thermal performance. A direct summary of this issue is provided in [18]. The same interest in cooling superconducting magnets also extends to helium PHPs [19].

Although the difference of thermal performance between the vertical or horizontal cryogenic PHP may be deduced from the above publications, in a practical application of PHPs in a superconducting magnet, the route extending between the cryocooler and the magnet will include both horizontal and vertical sections. A significant question that to date remains unanswered is to what extent the relative lengths of the vertical and horizontal sections will determine overall thermal performance of the PHP. The present study therefore provides a first attempt to answer this practical question and to thereby provide guidance in the application of cryogenic PHPs for the thermal design of superconducting magnet systems.

In order to characterize the dependence of PHP conductance on the relative extent of vertical and horizontal lengths, experiments have been designed and carried out to measure the thermal conductance (or thermal resistance) on a set of PHPs with identical geometries except for their varying aspect ratios where aspect ratio is defined by the length of the vertical adiabatic section divided by the length of the horizontal adiabatic section. The measurements have been carried out using the same hardware but at different times with helium or hydrogen as the working fluid.

2. Experimental setup

The PHP (Fig. 2) is constructed of 304 stainless steel tube, whose inner and outer diameters are 0.5 mm and 0.8 mm, respectively. The PHP includes three sections: the evaporator section where heat is applied, the adiabatic section, and the condenser section where heat is extracted by the cryocooler cold head. Both the evaporator section and the condenser section are soldered to separate copper plates, whose sizes are the same: 111.3 mm × 76.2 mm × 3.3 mm. In this study, there are four turns at each end of the PHP providing a total of 8 tubes extending between the evaporator and condenser sections. The lengths of the evaporator section and the condenser section are each 111.3 mm, while the length of the adiabatic section is 1000 mm. As shown in Fig. 2, the PHP is bent to a 90-degree angle at a location in the adiabatic section, and the resulting aspect ratio (α) is determined from the length of the vertical adiabatic section divided by the length of the horizontal adiabatic section.

Due to the low thermal conductance of the 8 parallel stainless-steel tubes, cooling the evaporator end of the PHP from room temperature to 4 K or even 20 K can take a very long time. To mitigate the problem, a set of 4 copper wires with a diameter of 1 mm were permanently connected between the evaporator copper plate and the condenser copper plate in order to speed up the cool down process of the PHP. For a later comparison it will be of value to note here that the thermal resistance between the evaporator and condenser plates, when the PHP is cooled to 4 K (or 20 K) and charged to a 50% fill ratio with the quiescent cryogen is 459 K/W (or 123 K/W).

The experimental test rig built to characterize the effects of different PHP aspect ratios is shown in Fig. 2a and Fig. 3. The PHP is enclosed in a vacuum chamber. The cooling source is a pulse tube cryocooler (CRYOMECH PT410) whose cooling capacity is 1.0 W at 4.2 K / 40 W at 45 K. The first-stage cold head of the cryocooler is connected to the aluminum radiation shield, and the second-stage cold head is connected to the condenser section through a copper bridge. During the experiment, a pump set is used to maintain a high vacuum in the vacuum chamber. The parasitic heat leak to the PHP when it is at 4 K, due to conduction and radiation is estimated at 18 mW. The high-pressure gas cylinder, buffer tank, and another set of pumps are used to purge and fill the PHP to a specified filling ratio. A resistive trim heater mounted on the condenser plate enables the temperature there to be controlled at 4.2 K for the helium tests and at ~ 20 K for the hydrogen tests.

The experiment utilizes six uncalibrated thermometers (SCIENTIFIC INSTRUMENTS RO-600), one on top of the radiation shield, one on the copper bridge near the second-stage cold head, two on the evaporator section, and two on the condenser section. In the uncalibrated version, the accuracy of the Ruthenium-oxide thermometer as reported by the Scientific Instruments, is +/- 0.2 K at 4.2 K and +/- 1.0 K at 20 K. However, for the purpose of accurately measuring ΔT, thermometers were selected as a matched group, so that the temperature variations between the thermometers subsequently mounted on the condenser and evaporator recorded identical temperatures to within +/- 0.08 K at 4.2 K and +/- 1.0 K at 20 K. Two pressure transmitters (OMEGA PX119-100AI) at room temperature are connected via thin capillary tubes to both ends of the adiabatic section. They are used to determine the filling ratio and measure the pressures in the evaporator and condenser ends while the PHP is operating. A resistive heater is mounted on the evaporator section to control the heat load. Two digital multimeters are used to measure the current (Tenma model 72–2050) and voltage (Fluke model 115) of the heater, and the product of the two is used to determine

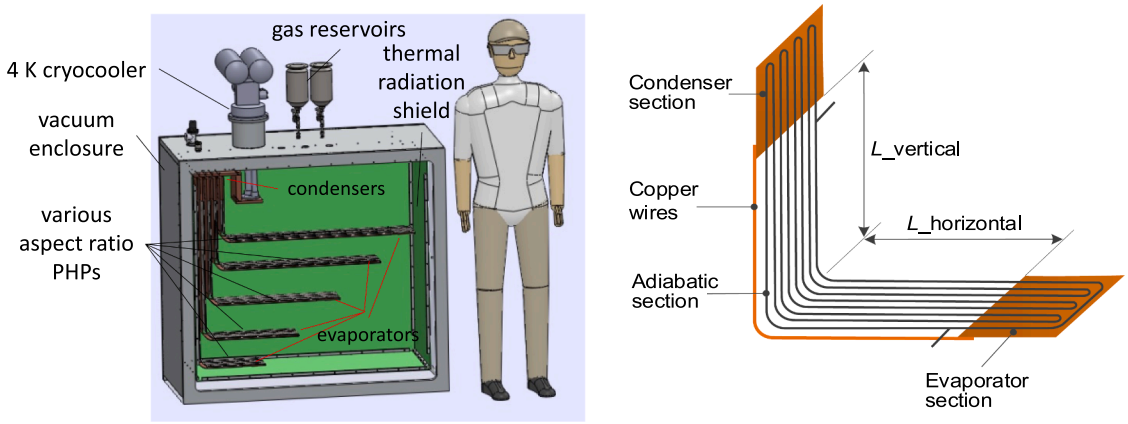

Fig. 2. a) Cryogenic PHP test rig. b) Schematic of the PHP with the aspect ratio $\alpha = L\_vertical/L\_horizontal$.

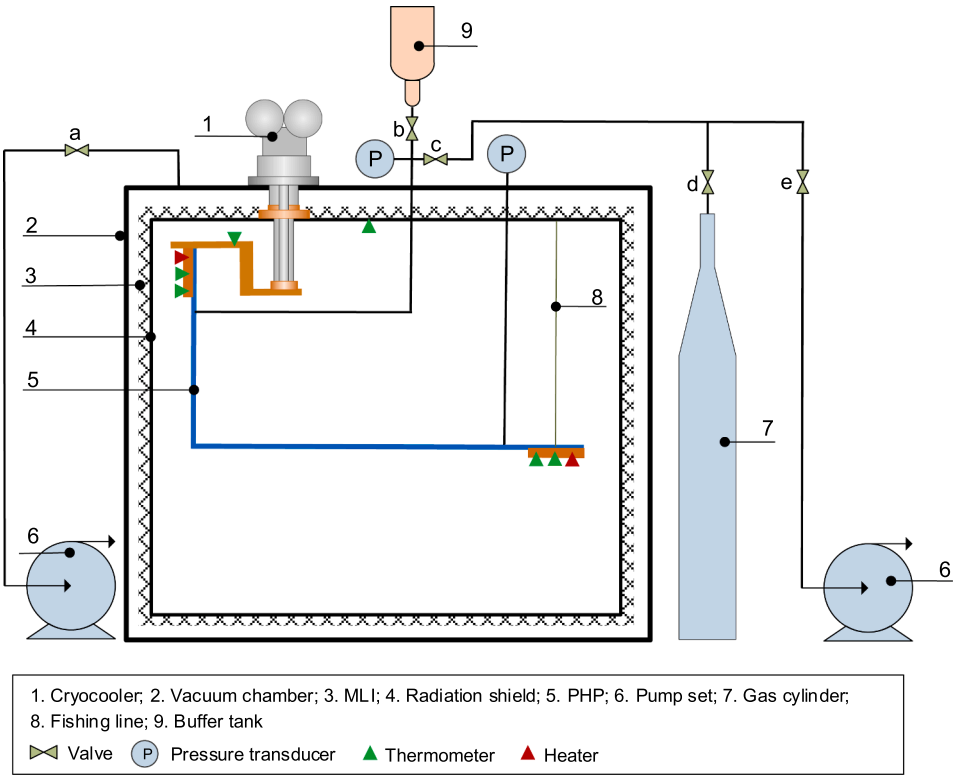

Fig. 3. Schematic of experimental apparatus.

the heat load. The identical heater installed on the condenser section is also used to accelerate the warm-up process for the PHP after completing a set of experiments.

2.1. Measurement approach and uncertainties

A sequence of procedures is required to conduct the pulsating heat pipe experiment in the cryogenic temperature region, and these are illustrated in Fig. 4. The first step, prior to any others, is to confirm the integrity of the instrumentation and data acquisition system at room temperature and ambient pressure. In this step electrical continuity is verified for all the thermometers, heaters, and pressure transducers. As necessary for cryogenic experiments, the next crucial step is to evacuate the vacuum vessel (item 2 in Fig. 3) while at room temperature, monitor the vacuum level, and confirm the absence of any leaks. In keeping with standard procedure for cryogenic experiments, a helium mass spectrometer based leak detector is used to confirm the absence of any leaks at a sensitivity level better than 10^{-8} atm-cc/sec.

A satisfactory vacuum level, to achieve the optimal insulation value of the multi-layer-insulation (MLI) is below 10^{-2} Pa.

Before charging the PHP with helium or hydrogen, the buffer tank and the PHP are purged three times to eliminate any residual gas. Then, the valves b, c and d are opened, and the buffer tank and PHP are filled with the helium or hydrogen gas to the pressure P_1. Next, valves c and d are closed, and the cryocooler is turned on. Pressure decreases with decreasing temperature. When the pressure is reduced to P_2, valve b is closed. Subsequently, the pressure of the buffer tank remains constant at P_2, while the pressure of the PHP continues to decrease with temperature. Finally, the PHP is allowed to stabilize at a minimum temperature of 2.9 K (18.7 K) for the helium (hydrogen) tests. Stable or steady state conditions following the cool down process are recognized when the condenser and evaporator temperatures remain constant to within +/- 0.01 K at 2.9 K and +/- 1 K at 18.7 K for more than 10 min. The helium (hydrogen) in the buffer tank and in the pipe connecting the PHP to room temperature is assumed to behave as an ideal gas, while the gas in the PHP is saturated. The filling ratio (FR) is defined as the ratio of the liquid volume to the total PHP volume, which can be derived from the following mass conservation equation:

$$\frac{P_1(V_{BT}+V_{CP}+V_{PHP})}{R_g T_{amb}} = \frac{P_2 V_{BT}}{R_g T_{amb}} + \frac{P_{sat} V_{CP}}{R_g T_{CP}} + \rho_l(FR \bullet \mathrm{V_{PHP}}) + \rho_v(1-\mathrm{FR})\mathrm{V_{PHP}} \quad (1)$$

where V_{BT}, V_{CP}, and V_{PHP} are the volumes of the buffer tank, connecting pipe, and PHP, respectively. R_g is the appropriate ideal gas constant. T_{amb} and T_{CP} are the temperatures of the buffer tank and the connecting pipe, respectively. T_{CP} is calculated as the average of the ambient temperature and the PHP condenser temperature. P_{sat} is the saturation pressure at the filling temperature of 2.9 K (18.7 K), while ρ_l and ρ_v are the densities of saturated liquid and vapor, respectively at that same temperature.

As an example of using Eq. (1) to determine a filling ratio, the value

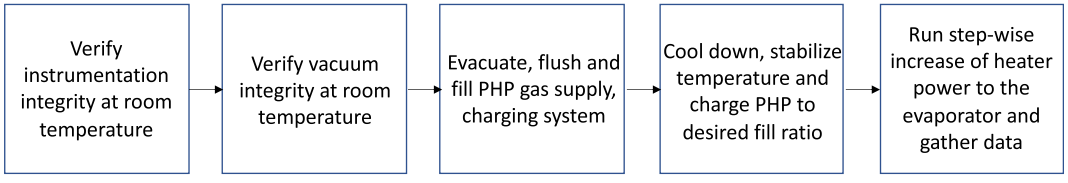

Fig 4. Test procedure sequence for cryogenic PHP measurements.

for each of the necessary parameters is shown in Table 1, along with the result of FR = 57% at 2.9 K.

Upon reaching steady state conditions following the cooldown and filling process, a sequence of stepwise increasing heat loads is applied to the heater mounted on the evaporator end of the PHP. At each value of applied load, a period of from 30 to 40 min is used to gather and average the measurements at the new steady state conditions. As shown in Fig. 5 below, temperatures reach new steady state values typically within ten minutes. Here 'steady state' is recognized by the condition when the evaporator temperature varies less than 0.02 K from its time-averaged value calculated over the preceding five-minute window.

Temperatures on the evaporator and condenser are controlled and measured using a Cryocon 24C temperature controller / monitor that incorporates a 15 Hz clock, 24 bit analog-to-digital converter and internal averaging.

Pressure measurements utilize 4–20 mA based devices powered by a 24 VDC Murr Electronik model MCS10-115–230/24 supply along with a 237 Ω-1% resistor. Power supplied to the heaters is measured using a Fluke model 115 multimeter for the voltage and Tenma model 72–2050 multimeter for the current supplied to the heaters.

National Instruments "Labview" software is used to gather and average 10 samples each of the temperature, and pressure signals once every second. Measurements are recorded at 5 s intervals. A summary of the instrumentation and associated meters is provided in table 2.

2.1.1. Uncertainty analysis

Thermal resistance values are calculated by the relation:

$$R_{thermal} = \frac{T_{evap} - T_{cond}}{\dot{Q}_{evap} + \dot{Q}_{parasitic}} \tag{2}$$

The uncertainty in the values of $R_{thermal}$ result from the uncertainties of the temperature measurements, and those of the applied heat. Uncertainties for both the temperature and pressure measurements are determined by the standard approach taking into account both the statistical variations in the measurement of the sample, with associated uncertainty u_A, and the manufacturer's reported accuracy of a given measurement, with its associated uncertainty u_B. As an example, the combined uncertainty of one evaporator temperature value, based on the average of n samples, and the sensor uncertainty gives:

$$\overline{T}_{evap} = \frac{1}{n}\sum_{k=1}^{n} T_{evap,k} = 5.57K \tag{3}$$

from which we have:

$$u_A\left(\overline{T}_{evap}\right) = \sqrt{\frac{1}{n(n-1)}\sum_{k=1}^{n}\left(T_{evap,k} - \overline{T}_{evap}\right)^2} = 0.010K \tag{4}$$

For a normal distribution, the sensor uncertainty provided by the manufacturer (±0.2 K) may be associated with three times the standard deviation in a sample of measurements. Then

$$u_B\left(\overline{T}_{evap}\right) = \frac{0.2}{3} = 0.067K \tag{5}$$

The combined uncertainty, then becomes

$$u_c = \sqrt{u_A\left(\overline{T}_{evap}\right)^2 + u_B\left(T_{evap}\right)^2} = \sqrt{0.01^2 + 0.067^2} = 0.068K \tag{6}$$

so that the measured value is: $T_{evap} = 5.57 \pm 0.068K$.

Table 1
Parameters for obtaining filling ratio (helium).

P_1 (kPa)	P_2 (kPa)	P_{sat} (kPa)	V_{BT} (m^3)	V_{CP} (m^3)	V_{PHP} (m^3)	T_{amb} (K)	T_{CP} (K)	ρ_l (kg/m3)	ρ_v (kg/m3)	FR (-)
297.2	207.7	20.63	1.11E-03	7.9E-07	1.978E-06	300	151.5	142.1	3.9	57% at 2.9 K

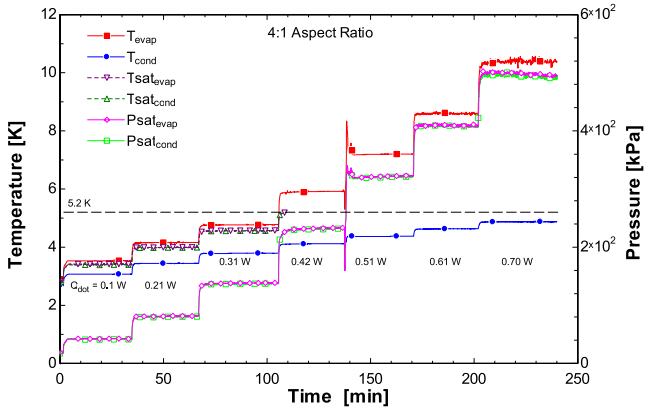

Fig. 5. Temperature and pressure data obtained with the 4:1 aspect ratio helium PHP. The horizontal dashed line identifies helium's critical temperature of 5.2 K.

Table 2
Summary of Instrumentation and Measurement Techniques.

Measurment	Sensor	Meter	Comments
T_{evap}	RO600 (SI)	Cryocon 24C	4-wire resistance
T_{cond}	RO600 (SI)	Cryocon 24C	4-wire resistance
Pressure	OMEGA PX119-100AI	Murr Electronik MCS10-115–230/24	4–20 mA signal across a 237 Ω – 1% resistor
Heater	Voltage	FLUKE 115 multimeter	4-wire method
Heater	Current	TENMA 72–2050	4-wire method

Two measurements of the condenser temperature result in a slightly lower uncertainty for those values (~ ± 0.047 K). Single measurements of the heater current and voltage are combined with the temperature uncertainties and standard uncertainty propagation methods to determine the overall uncertainty in the thermal resistance calculated from Eq. (2). The parasitic heat load, determined from measured temperatures with no power supplied to the heaters is found to be less than 20 mW. The uncertainties in both the thermal resistance and applied heat load are reflected by the error bars in Figs. 6–8, and 10–13.

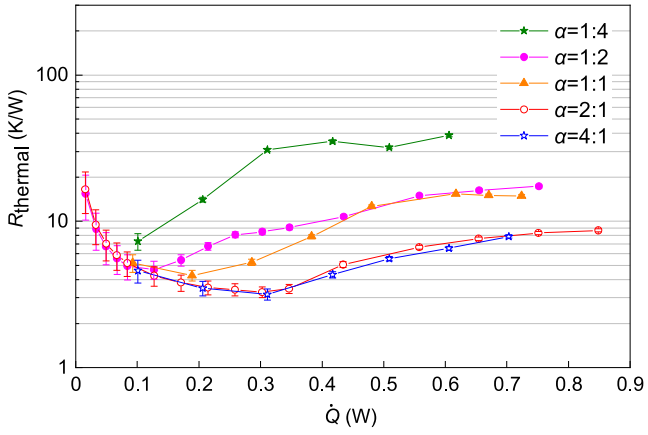

Fig. 6. Thermal resistance data for the helium PHPs.

3. Results and discussion

The same PHP was tested under different aspect ratios of 1:4, 1:2, 1:1, 2:1 and 4:1 for both helium and hydrogen. At each aspect ratio, the heat load of the evaporator section is gradually increased from zero up to a value close to the cryocooler's maximum cooling capacity. Each heat load is maintained over an extended time period (from 15 to 30 min) and then adjusted to allow the PHP to stabilize again at the new heat load. For the helium tests, the filling ratio is set to 56% −57% at 2.9 K, based on previous research of a helium PHP with a 1000 mm adiabatic section which demonstrated that a filling ratio close to 58% at 2.9 K is optimal [24]. Except for the fact that the PHP used in [24] was operated in the fully vertical orientation, all other aspects of the present PHP and that used in [24] are the same including the diameter, wall thickness, and material of the capillary tubes, the 1000 mm adiabatic length, the fill ratio and the range of applied heat load. The measurements obtained with hydrogen used two different filling ratios, 50% and 70%. The data and implications from the helium and hydrogen tests are provided separately and sequentially in the following sections.

3.1. Helium measurements

3.1.1. Cooling the PHP to 4 K

Although the cool down process observed during these measurements is determined by the specific configuration and components used in the test, it is worth noting that the PHP does not provide any thermal advantage to the cool down process. Indeed, due to the stainless steel capillary used to form this particular PHP, the thermal resistance between the condenser and evaporator ends is very substantial and results in a significant lag between the temperature decrease of the condenser and that of the evaporator. As mentioned above, a limited number of copper wires were added between the two ends of the PHP to enhance the evaporator cool down. As a result of the modification, both the condenser and evaporator plates cooled to ~ 5 K within 17 h, while the aluminum thermal radiation shield, due to its larger thermal mass, required an additional 23 h to reach its final equilibrium temperature of 50 K. By the time that the thermal shield reached its final temperature, the evaporator and condenser plates had also cooled to their coldest temperature, near 2.9 K. At the steady state condition following cool down, the saturation temperature of the helium contained in the condenser and evaporator ends of the PHP, based on the respective measured pressures were 2.36 K and 2.51 K. In this equilibrated condition, a noticeable temperature difference exists between the copper plates at either end of the PHP and the corresponding fluid temperature inside, presumably from the parasitic heat loads at each end.

Stainless steel has frequently served as the material of choice for PHP construction, primarily to highlight the huge increase in heat transfer between the evaporator and condenser ends when the PHP is charged with the working fluid and operates. However, alternative materials such as copper-nickel would be suitable for constructing the small diameter tubing and would also provide the advantage of a more favorable conductance between the two ends even before the tubing is filled with the working fluid.

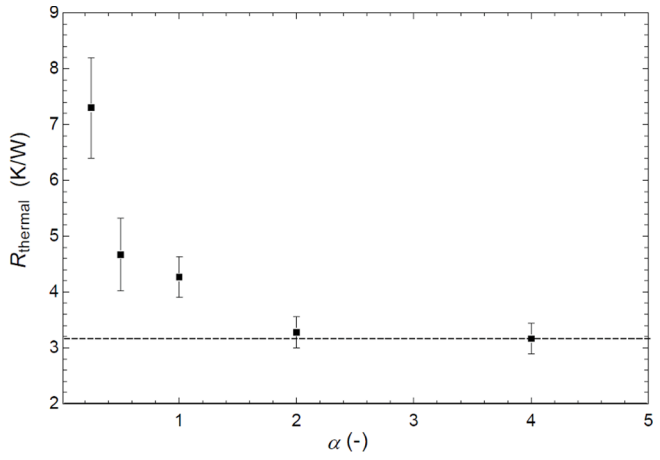

Fig. 7. Minimum thermal resistance vs. aspect ratio (α) for the 8-tube helium PHPs.

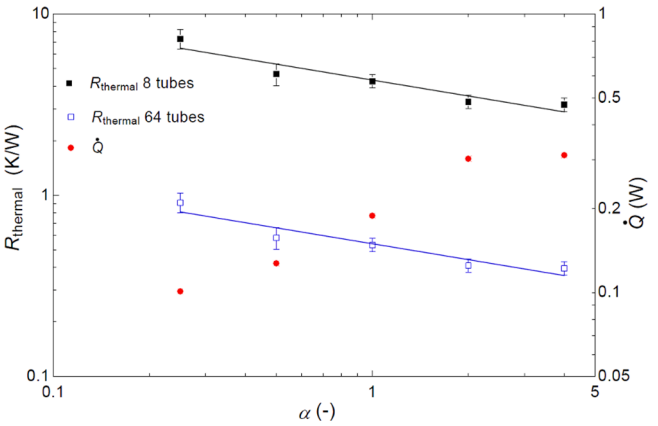

Fig. 8. Minimum thermal resistance values for a single 8-tube and eight parallel 8-tube helium PHP.

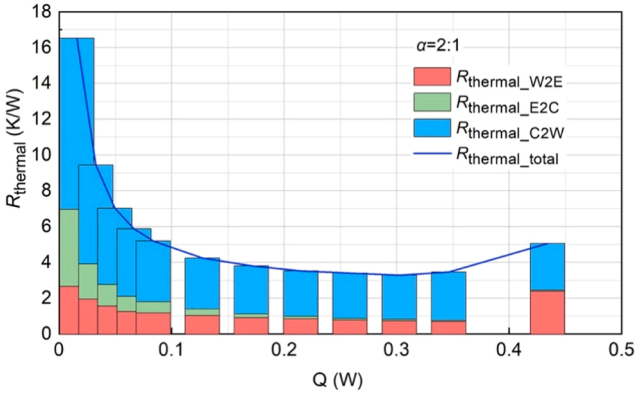

Fig. 9. Thermal resistance contributions. $R_{thermal\_W2E}$ – thermal resistance from the wall to the fluid in the evaporator, $R_{thermal\_E2C}$ – thermal resistance from evaporator fluid to condenser fluid, $R_{thermal\_C2W}$ – thermal resistance from condenser fluid to the wall.

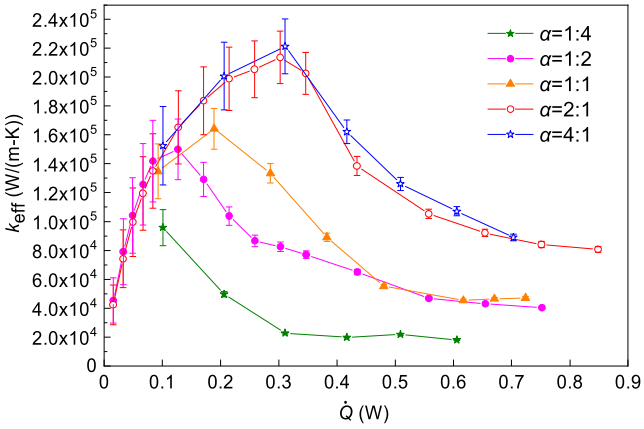

Fig. 10. Effective thermal conductivity for the 8-tube helium PHPs with varying aspect ratio.

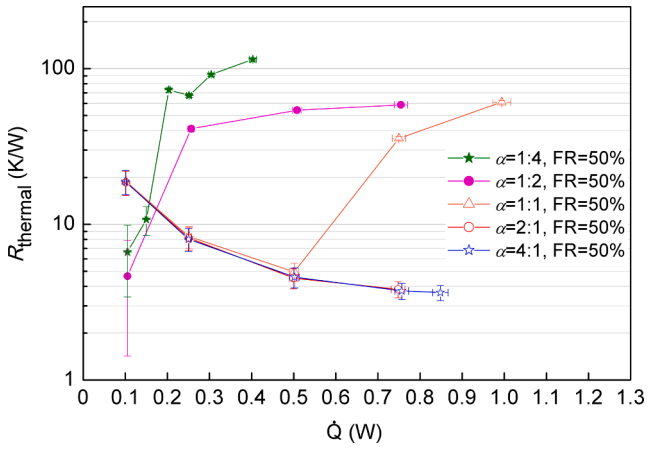

Fig. 11. Thermal resistance of the hydrogen PHP with a 50% fill ratio.

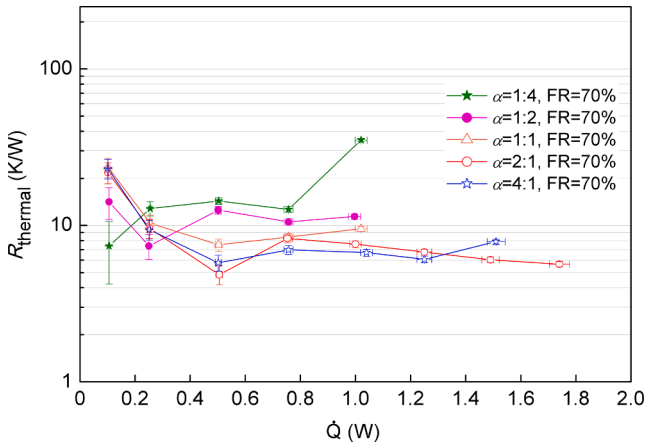

Fig. 12. Thermal resistance of a hydrogen PHP with a 70% fill ratio.

3.1.2. *Temperature and pressure curves*

In keeping with the anticipated dependence on orientation, the helium PHP provided the best thermal performance when the majority of its length was in the vertical orientation. A record of the temperatures and pressures gathered for the 4:1 aspect ratio is shown in Fig. 5. Here, the spatially averaged temperatures for the evaporator and condenser are shown along with the measured pressures in the evaporator and condenser as well as the corresponding saturation temperatures. The heat load applied to the evaporator end is identified at each step in the data. Saturation temperatures are not recorded for any values higher than the critical temperature of helium, 5.2 K, since they are not linked to the measured pressure in the supercritical region. At all heat loads, the difference in pressure between the evaporator and condenser ends is less than 1500 Pa.

In the case of the 4:1 aspect ratio, the maximum temperature measured in the evaporator region approaches 11 K and indicates that the fluid at the evaporator end no longer contains liquid, but rather supercritical helium. It is significant to note that the helium PHP continues to function under these conditions and is effective at transporting heat. For the smaller aspect ratio configurations, comprised of a larger horizontal section, the evaporator temperature at the maximum heat load increases; thus, at an aspect ratio of 1:4, the evaporator temperature approaches 28 K while the condenser maintains a temperature below the critical temperature of 5.2 K.

3.1.3. *Thermal resistance*

The heat transfer characteristic of the helium PHP is best represented in terms of its thermal conductance (in units of W/K) or equivalently its thermal resistance (in units of K/W), as a function of the applied heat load. Fig. 6 displays the thermal resistance of the five helium PHPs measured in this investigation as a function of the applied heat load at the evaporator end.

A number of important observations can be obtained from the thermal resistance data obtained in the helium PHP:

- The thermal resistance is lowest for the helium PHP with the largest aspect ratio. With$\alpha = 4$ a minimum thermal resistance of 3.2 K/W is measured, and the resistance increases to 7.3 K/W when α=¼. The ratio of these values is similar to that of fully vertical and fully horizontal helium PHPs.
- The minimum thermal resistance of the helium PHP varies with the applied heat load. Furthermore, the value of the applied heat corresponding to the minimum thermal resistance decreases with the aspect ratio. In the data presented in Fig. 6, the heat load associated with the minimum thermal resistance decreases from 0.3 W to 0.1 W, as the aspect ratio decreases from 4 to ¼.
- A summary of the influence of the aspect ratio on the minimum thermal resistance gathered for the helium PHP is shown in Fig. 7 and Fig. 8. Fig. 7 reflects the expected dependence of $R_{thermal}$ on the aspect ratio and one may associate the limiting values of 3 K/W and 7.3 K/W observed in this study as approaching the asymptotes associated with a fully vertical [24,25] and fully horizontal [19,26] helium PHP, respectively.
- The log–log representation of the minimum thermal resistance data shown in Fig. 6 reveals that within the range of aspect ratios used in the present study, the minimum thermal resistance scales as $c \cdot \alpha^{-0.3}$ where $c = 4.32$ when the PHP is comprised of 8 parallel tubes. The associated heat load for each thermal resistance is also displayed.
- The blue line included in Fig. 8 is a projection of the PHP behavior to conditions that were not directly measured; they are extrapolated

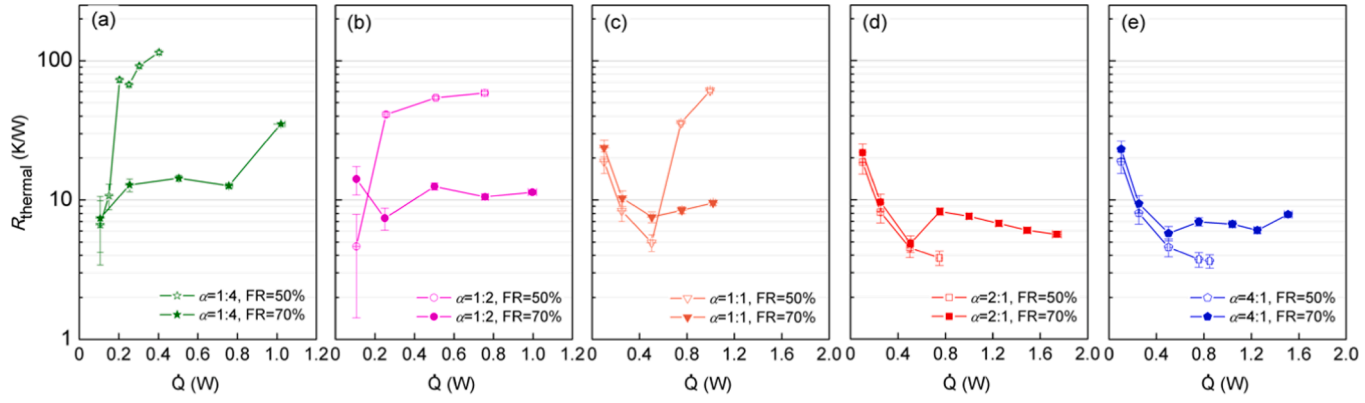

Fig. 13. Thermal resistance of hydrogen PHPs with 50% and 70% fill ratio as a function of heat load for various aspect ratios: a) 1:4, b) 1:2, c) 1:1, d) 2:1, and e) 4:1.

based on the scaling behavior described by Xu, Li, and Liu [27]. The line is presented to demonstrate that it is possible, with the use of PHPs, to obtain thermal resistance values less than 1 K/W. It is important for those designing superconducting magnet systems to recognize this feature, so that they may readily include helium PHPs as reliable, low resistance thermal components. As shown by Xu, Li, and Liu [27] the thermal conductance (or resistance) of multiple n-turn-PHPs connected in parallel will increase in proportion to the number of n-turn-PHPs connected in parallel and thus scale with the total cross-sectional area of the tubes. The blue line displayed in Fig. 8 reflects the expected performance of eight helium PHPs identical to the ones used in this study, connected in parallel between the condenser and evaporator plates. In such a case the combined PHPs would provide 64 parallel tubes and the overall thermal resistance would be decreased by a factor of 8 compared to the measured values displayed in Fig. 7 for each of the applied heat load values. With the eight parallel PHP configuration the thermal resistance for the 1:4 aspect ratio is 0.91 K/W decreasing to 0.4 K/W for the aspect ratio of 4:1.

- The minimum thermal resistance of the helium PHP in each configuration occurs at a specific value of the applied heat. That is, there exists an optimal heat load that corresponds to the minimum thermal resistance. In the studies conducted here, the heat load associated with the minimum thermal resistance ranges between 0.1 W and 0.3 W. Optimally designed current leads display a similar feature [28]. That is, their geometry (aspect ratio) is typically designed to correspond to a minimum thermal penalty (W/kA) at the full, steady state, operating current. At current levels greater or less than the maximum design value, the heat load per current is larger than the optimized value. The PHP should also be designed for optimal operating conditions and will in that case provide a minimum thermal resistance.

3.1.4. Contributions to the thermal resistance

Fig. 9 displays thermal resistance information associated with the 8-tube helium PHP that has an aspect ratio of 2. Assuming that the saturation temperatures generated from the measured pressures in the condenser and evaporator ends reflect the fluid temperatures in those regions, a thermal resistance between the copper plates and the fluid inside the PHP may be obtained. Fig. 9 suggests that the majority of the thermal resistance between the evaporator and condenser occurs at the solid–fluid interface, and that a much smaller thermal resistance is associated with the temperature difference in the helium between the same two ends. For example, in this case the minimum thermal resistance in the helium is 48 mK/W with a heat load of 0.43 W. The larger thermal resistance of the plate and wall at the condenser end can in part be attributed to the temperature-dependent thermal conductivity of copper and stainless steel in the liquid helium range. For example, the thermal conductivity of copper at 6 K is 45% larger than at 4 K. Thus, the thermal resistance of the condenser plate is expected to be larger than the thermal resistance of the evaporator plate. A similar increase in the thermal conductivity of 304 stainless steel occurs in this temperature range, so that the thermal resistance of the condenser wall will also be larger than the thermal resistance of the evaporator wall. Without information regarding velocities, heat transfer coefficients and flow characteristics, a more quantitative analysis regarding this feature is not possible.

3.1.5. Effective thermal conductivity

The thermal performance of PHPs is frequently expressed in terms of an effective thermal conductivity (k_{eff}), which is calculated as

$$k_{\text{eff}} = \frac{QL_{\text{eff}}}{A\Delta T} \tag{7}$$

where Q is the heat load, L_{eff} is the distance between the evaporator midpoint and the condenser midpoint, A is the total cross-sectional area of the fluid in the parallel tubes, and ΔT is the temperature difference between the evaporator and condenser. Fig. 10 displays the effective thermal conductivity values for each of the five PHPs as a function of the applied heat load with the aspect ratio as a variable parameter. Here the maximum effective thermal conductivity values vary from 10 kW/m-K to over 220 kW/m-K. Although these values are amazing in comparison with pure metals such as copper or aluminum, for practical applications such as cooling components in a superconducting magnet, the thermal conductance results shown in Figs. 7–9 provide better guidance for design activities.

3.2. Hydrogen measurements

The testing procedure when using hydrogen as the fluid in the PHP was very similar to that when using helium, except that the controlled temperature on the condenser plate was maintained between 19 K and 20 K. Because the cooling capacity of the cryocooler is significantly larger at 20 K (~6 W) than at 4.2 K (1 W), in the hydrogen tests it was possible to maintain a constant temperature on the condenser plate by reducing the heat applied to the trim heater on the condenser plate as the heat load to the evaporator plate was increased. As with the helium tests, the heat applied at the evaporator plate was increased in a stepwise fashion and held constant for 30–60 min in order to confirm steady-state conditions. 'Steady state' for the hydrogen data is recognized by the condition when the evaporator temperature varies less than 0.25 K from its time-averaged value calculated over the preceding five-minute window. In most cases, the test was halted when the evaporator temperatures approached or exceeded hydrogen's critical temperature of 33 K. Each of the stepwise group of measurements for a given aspect ratio and fill ratio were conducted one time.

The cool-down time to reach 20 K on the PHP and an equilibrium temperature of 58 K on the thermal shield was 11 h and 39 h, respectively. These times are similar to those realized during the cool down to 4.2 K because of the relatively minor enthalpy difference of the cold mass between 20 K and 4.2 K.

3.2.1. Data gathered with a 50% fill ratio

A composite graph of the thermal resistance for the hydrogen PHPs with a fill ratio of 50% as a function of the applied heat load with the aspect ratio as a variable parameter is shown in Fig. 11.

Notable features of the data are as follows:

- The larger aspect ratio PHPs display a smoothly decreasing thermal resistance as the heat load is increased, falling to 3.6 K/W at a heat load of 0.8 W.
- The thermal resistance data roughly fall into two separate branches, one associated with the higher aspect ratio configurations displaying smoothly decreasing values of the thermal resistance as the heat load increases, and a second for the configurations with aspect ratios ≤ 1 in which the thermal resistance trends toward the quiescent fluid limit of 123 K/W. The data suggest that large portions of the horizontal segments toward the evaporator end in the low-aspect-ratio PHPs are vapor locked and produce very little if any fluid motion to effectively transfer heat.

3.2.2. Data gathered with a 70% fill ratio

When the hydrogen PHP is initiated with a 70% fill ratio and subject to the same stepwise increase of heat loads to the evaporator, the resulting thermal resistance values are larger than those obtained for the high-aspect-ratio, high-heat-load cases with a 50% fill ratio, but they remain relatively constant over the complete range of heat loads. Furthermore, the thermal resistance values are also relatively insensitive to variations in the aspect ratio. This behavior is displayed in Fig. 12.

Prior reports [7,19] demonstrate that as the fill ratio for a helium PHP increases above 60%, random temperature excursions and thermal noise in the evaporator, which exist with lower fill ratios, are greatly

diminished or completely absent. Although it is extremely difficult in a cryogenic PHP to visually observe the flow patterns, one may conjecture that the relatively constant thermal performance with the 70% fill ratio is due to the sustained presence of liquid slugs in the evaporator region for all the various aspect ratio configurations and applied heat loads.

The same thermal resistance data that was provided in Fig. 11 and Fig. 12, is also displayed in Fig. 13 but it is described separately for each of the aspect ratio configurations in order to highlight the significant difference between the performance of the 50% fill ratio and 70% fill ratio cases over the complete heat load range.

From the 50% fill ratio data displayed in Fig. 11 one finds a favorable decrease in thermal resistance by a factor of five as the applied heat load increases from 0.1 W to 0.9 W for the largest aspect ratio configurations. However, over the entire range of aspect ratio and heat load space, the variation of thermal resistance by two orders of magnitude significantly degrades the value of the PHP as a reliable heat transfer component in a superconducting magnet design. In contrast, variations of the thermal resistance with a 70% fill ratio remain between 5 K/W and 30 K/W over the entire range of aspect ratios and applied heat load. Furthermore, 87% of the data display thermal resistance values ranging between 5 K/W and 15 K/W. Such consistent thermal performance is crucial for applications in superconducting magnet designs. It provides the important feature of reliability for system designs that depend on the thermal conductance between a heat source and the heat sink typically provided by a cryocooler.

If a lower thermal resistance than displayed in Fig. 12 is required, multiple PHPs of the same geometry can be used to connect the magnet (or thermal shield) to the cryocooler. For example, eight such hydrogen PHPs would bring the overall thermal resistance down to or below a thermal resistance of 1 K/W. The crucial design feature would be to ensure a fill ratio of 70%.

4. Conclusions

The experimental activities reported herein for both helium and hydrogen PHPs characterize the influence of the aspect ratio, which is the ratio of vertical to horizontal lengths, on their heat transfer performance. Due to the anticipated convoluted pathway that a PHP will need to traverse between the cold tip of a cryocooler and the surface of a superconducting magnet, the results provide a significant means to judge the influence of vertical and horizontal lengths on the overall thermal performance. Results presented in this report provide the first characterization of the influence of aspect ratio on thermal performance for helium and hydrogen pulsating heat pipes. The results provide crucial information to those designing superconducting magnets in two forms. First, they demonstrate that helium and hydrogen PHPs can provide a thermal path with a resistance less than 1 K/W. Secondly, the results define the appropriate conditions for optimal performance; in terms of applied heat load (0.1 W – 0.3 W) for helium PHPs, and in terms of fill ratio (70%) for hydrogen PHPs.

The data further reveal that the overall thermal resistance for the helium PHP decreases as the geometry transitions from vertical to horizontal, which is in keeping with the published limits of fully vertical and fully horizontal configurations. Moreover, the measured thermal performance of the five different aspect ratios for the 8-tube configuration included in this study reveal that the minimum thermal resistance for helium PHPs varies smoothly as $R_{thermal} = 4.32\alpha^{-0.3}$ (K/W) in the range of $0.25 \leq \alpha \leq 4$. Based on the known dependence of overall thermal resistance as a function of the total cross-sectional area of the fluid within the parallel tubes, one can project that a configuration utilizing eight identical PHPs operating in a parallel configuration would result in a minimum thermal resistance $R_{thermal}=0.54\alpha^{-0.3}$ (K/W) over the same range of α and for the same range of applied heat load, that is from 0 W to 1 W.

The combination of pressure and temperature measurements in this study has enabled a breakdown analysis of the thermal resistance between the evaporator and condenser. The data reveal that the majority of thermal resistance occurs between the copper plate and fluid at each end of the PHP, suggesting that future improvements in materials preparations and fabrication methods, such as roughened or extended surface to increase the surface area, could further reduce those thermal resistance contributions.

Results from the hydrogen PHP data reveal that for purposes of consistent thermal resistance values in the design of a superconducting magnet system, the PHP should be initiated with a fill ratio of 70%. For a hydrogen PHP, a fill ratio of 70% significantly reduces the influence of orientation and heat load on the PHP's thermal resistance compared with that experienced with lower fill ratios. Incorporating a hydrogen PHP with a fill ratio of 50% will introduce significant uncertainty (two orders of magnitude variation) in the components' thermal transport performance.

In summary, the thermal transport characteristics of the PHP enable a reduction in thermal mass and a large increase in effective thermal conductivity compared to the pure metals typically used for cryogenic thermal bus components such a copper and aluminum. The small size of the capillary tubing however limits the conductance of the PHPs; thus multiple units configured in parallel are required in order to reduce the associated thermal resistance below 1 K/W. Considering its low mass, passive and large heat transfer capabilities, the PHP can provide a valuable component in the overall optimal thermal design for a superconducting magnet system.

Declaration of Competing Interest

The authors declare that they have no known competing financial interests or personal relationships that could have appeared to influence the work reported in this paper.

Acknowledgement

This work is supported by the U.S. Department of Energy, Office of Science under award DE-SC-0019920. Xiao Sun acknowledges the scholarship during her study in the University of Wisconsin-Madison from the China Scholarship Council.

References

[1] T Mito, K Natsume, N Yanagi, H Tamura, T Tamada, K Shikimachi, N Hirano, and S. Nagaya, "Development of Highly Effective Cooling Technology for a Superconducting Magnet Using Cryogenic OHP." IEEE Transactions on Applied Superconductivity vol.20: pp. 2023–6, (2010).
[2] K. Natsume, T. Mito, N. Yanagi, H. Tamura, T. Tamada, K. Shikimachi, N. Hirano, S. Nagaya, Heat transfer performance of cryogenic oscillating heat pipes for effective cooling of superconducting magnets, Cryogenics 51 (2011) 309–314.
[3] T. Mito, K. Natsume, N. Yanagi, H. Tamura, T. Tamada, K. Shikimachi, N. Hirano, S. Nagaya, Achievement of high heat removal characteristics of superconducting magnets with imbedded oscillating heat pipes, IEEE Trans. Appl. Supercond. 21 (2011) 2470–2473.
[4] M.N. Wilson, Superconducting Magnets, Clarendon Press, Oxford, 1983.
[5] Cryocoolers (vols 6-21), S.D. Miller & R.G. Ross, Jr., Eds, ICC Press, 1991–2021.
[6] https://www.cryomech.com/cryocoolers/.
[7] Y.M. Dai, L.G. Yan, Q.L. Wang, B.Z. Zhao, S.S. Song, Y.Z. Lei, H.S. Wang, H. Wang, S.Z. Chen, J.S. Cheng, Fabrication of a 10 Tesla Cryogen Free Superconducting Magnet, IEEE Trans. Appl. Supercond. 21 (3) (2011) 1608–1611.
[8] S. Casalbuoni, A. Cecilia, S. Gerstl, N. Glamann, A.W. Grau, T. Holubek, C. Meuter, D. Saez de Jauregui, R. Voutta, C. Boffo, Th. Gerhard, M. Turenne, W. Walter, Characterization and Long Term Operation of a Novel Superconducting Undulator with 15 mm Period Length in a Synchrotron Light Source, Phys. Rev. Accelerators Beams 9 (2016) 11070.
[9] https://www.shicryogenics.com/products/cryocoolers/.
[10] https://www.arscryo.com/ps-cc-scm.
[11] L Dresner, Stability of Superconductors, Plenum Press, 1995. (see especially, pg. 71).
[12] Y.K. Iwasa, Case Studies in Superconducting Magnets, Design and Operational Issues, 2nd Edition, Springer, 2009.
[13] Joel Fuerst, Argonne National Laboratory, private communication (2018).
[14] G.F. Nellis, S.A. Klein, Heat Transfer, Cambridge University Press, 2009.

[15] L.D. Fonseca, J. Pfotenhauer, F. Miller, Results of a three evaporator cryogenic helium pulsating heat pipe, Int. J. Heat Mass Transf. 120 (2018) 1275–1286.
[16] X. Sun, S.Z. Li, B. Jiao, Z.H. Gan, J.M. Pfotenhauer, B. Wang, Q.Y. Zhao, D.L. Liu, Experimental study on hydrogen pulsating heat pipes under different number of turns, Cryogenics 111 (2020), 103174.
[17] P. Charoensawan, S. Khandekar, M. Groll, P. Terdtoon, Closed Loop Pulsating Heat Pipes Part A: Parametric Experimental Investigations, Appl. Therm. Eng. 23 (2003) 2009–2020.
[18] J.M. Pfotenhauer, Recent Developments in Cryogenic Heat Pipes, ES Energy Environ. 3 (2019) 1–3.
[19] M.N. Li, L.F. Li, D. Xu, Effect of Filling Ratio and Orientation on the Performance of a Multiple Turns Helium Pulsating Heat Pipe, Cryogenics 100 (2019) 62–68.
[20] Q. Liang, Y. Li, Q.L. Wang, Experimental investigation on the performance of a neon cryogenic oscillating heat pipe, Cryogenics 84 (2017) 7–12.
[21] Q. Liang, Y. Li, Q.L. Wang, Effects of filling ratio and condenser temperature on the thermal performance of a neon cryogenic oscillating heat pipe, Cryogenics 89 (2018) 102–106.
[22] Q. Liang, Y. Li, Q.L. Wang, Study on a neon cryogenic oscillating heat pipe with long heat transport distance, Heat Mass Transf. 54 (2018) 1721–1727.
[23] M. Barba, R. Bruce, F. Bouchet, A. Bonelli, B. Baudouy, Thermal Study of a one-meter long Neon Cryogenic Pulsating Heat Pipe, IOP Conference Series Mater. Sciency Eng. 502 (2019), 012152.
[24] L.D. Fonseca, J. Pfotenhauer, F. Miller, Short communication: thermal performance of a cryogenic helium pulsating heat pipe with three evaporator sections, Int. J. Heat Mass Transf. 123 (2018) 655–656.
[25] LD Fonseca, "Experimental Characterization of Cryogenic Helium Pulsating Heat Pipes" PhD Thesis, University of Wisconsin - Madison (2017).
[26] L.D. Fonseca, F.K. Miller, J.M. Pfotenhauer, A Helium Based Pulsating Heat Pipe for Superconducting Magnets, Adv. Cryog. Eng., AIP Conference Proceedings 1573 (2014) 28–35.
[27] D. Xu, L.F. Li, H.M. Liu, Effect of number of turns and configurations on the heat transfer performance of helium cryogenic pulsating heat pipe, Cryogenics 96 (2018) 159–165.
[28] J.E.C. Williams, Counterflow Current Leads for Cryogenic Applications, Cryogenics 3 (December 1963) 234–238.